Exploration of BioMat-X

Open Exploration

Open Access Original Article

# Ecologically facilitative green approach for synthesizing gold nanoparticles: a screening study of bioactivities

Sumaira Mumtaz[1*], Ietzaz Husain[2], Muhammad Javid Iqbal[3]

[1]Department of Chemistry, Faculty of Sciences, University of Agriculture, Faisalabad 38000, Pakistan
[2]Directorate of ITRCBD, University of Agriculture, Faisalabad 38000, Pakistan
[3]Department of Chemistry, COMSATS University Islamabad, Lahore 53700, Pakistan

***Correspondence:** Sumaira Mumtaz, Department of Chemistry, Faculty of Sciences, University of Agriculture, Agriculture University Road, Faisalabad 38000, Pakistan. smpieces@gmail.com
**Academic Editor:** Laichang Zhang, Edith Cowan University, Australia
**Received:** October 16, 2024 **Accepted:** May 22, 2025 **Published:** August 6, 2025

**Cite this article:** Mumtaz S, Husain I, Iqbal MJ. Ecologically facilitative green approach for synthesizing gold nanoparticles: a screening study of bioactivities. Explor BioMat-X. 2025;2:101343. https://doi.org/10.37349/ebmx.2025.101343

## Abstract

**Aim:** Plants possess tremendous medicinal properties which have been supposed to be promising candidates for biomedical applications, especially in the field of nanobiotechnology. To analyze one such view, the current study was adopted to synthesize gold nanoparticles (Au*nps) by employing the extract of *Murraya koenigii* (EMk) for the evaluation of phenolics, antioxidant, antimicrobial, hemolytic, and biocompatible activities.

**Methods:** The synthesis process was carried out in a single step by mixing EMk and gold salt (Au salt) solution and monitored using UV/Visible spectroscopy. The process was optimized via variation in environmental variables. Characterization techniques such as Fourier transform infrared (FTIR) spectroscopy, transmission electron microscopy (TEM), scanning electron microscopy (SEM), X-ray diffractometer (XRD), and energy dispersive X-rays (EDX) were employed. In vitro biological activities (total phenolic, antioxidant, antimicrobial, and hemolytic) using different concentrations of Au*nps along with EMk were assessed. An in vivo histopathology study on Wistar rats was analyzed.

**Results:** The band of Au*nps was observed at 540 nm, which showed successful synthesis. The FTIR spectra of Au*nps indicated the role of different functional groups (alkane, aromatic ester, thiol, nitro, and aldehyde) of EMk during synthesis. The TEM analysis illustrated a 50 nm size of Au*nps; SEM showed the presence of some aggregates; EDX represented elemental nature, and XRD proved the crystalline nature of these Au*nps. The Au*nps possessed significant phenolic content and displayed prominent antioxidant activities by quenching free radicals. Similarly, momentous inhibitory action was observed against microbial strains of *Escherichia coli* and *Bacillus subtilis*. The hemolytic study showed the least to non-toxic effect of these nanoparticles on red blood cells (RBCs) even at enhanced concentration. Histopathology study showed fair compatibility without inducing any apparent pathological lesions on the liver tissues of Wistar rats.

**Conclusions:** Plausibly, all the above investigations strongly emphasized the use of medicinal plant-based Au*nps for biological applications.

## Keywords

Aggregate, inhibition, microbial, nanoparticles, synthesis, antioxidant, biomedical

## Introduction

Nanotechnology is endlessly being engaged in the synthesis of nanomaterials that possess a size between the range of 1 to 100 nm for multiple applications, most notably, in the area of nanomedicine [1]. Owing to their multifaceted characteristics, metals such as silver, gold, platinum, titanium, copper, zinc, calcium, and iron have been used for synthesizing their nanoparticles for versatile practices [2]. The most important aspects of using metal nanoparticles are their unique physicochemical traits (electronic, magnetic, optical, and catalytic), which make them exclusive aspirants for sundry uses. That's why different fields such as physics, biology, chemistry, and engineering are gaining advantages by the use of these metal nanoparticles [3, 4]. Among transition metals, gold is one of the most precious metals possessing distinct features both in terms of physical and chemical properties, and has been extensively employed in the multidisciplinary research fields. Currently, gold nanoparticles (Au*nps) have been investigated in the medical field for drug delivery, diagnosis, bio-labelling, pathogenic identification, photothermal therapy, besides other valuable applications [5].

With the advent of drug-resistant microbial strains, the medicinal formulations require to shift in order to combat the drug resistance. Fatefully, metal nanoparticles have been employed in research work for the treatment of drug resistance microbes [6]. Similarly, the nanoparticles based formulated products should have ability to induce less toxicity and more biocompatibility for biological uses [7]. Outstandingly, the metal nanoparticles have a large surface area to volume ratio, besides a small size, which is suitable for biomedical purposes [8]. Moreover, the metal nanoparticles also possess significant effects as anticancer and antioxidant agents [9–11]. The development of any formulation for medicinal purposes requires non-toxicity or minimum harm to the biological entities when entering the body. One such study is based on the analysis of hemolytic activity. The RBCs may release hemoglobin into the surrounding medium in response to foreign invaders. Metal nanoparticles are supposed to have a non-toxic effect on RBCs due to their biocompatibility within the biological system.

Despite the fact that chemical and physical approaches are extensively in use for metal nanoparticles' synthesis [12]; however, these methods are associated with the involvement of high cost, energy, expensive chemicals, temperature, and time consumption [13]. Due to these reasons, biological ways have been gaining much attention for synthesis purposes in recent years [14, 15]. Although bacteria, fungi, algae, and yeast are included among biological sources, they require severe protocols to follow [16]. Reports have ascribed prominent features of plant extracts as green mean, which is cost-effective, simple, nontoxic, and quick [17]. Furthermore, single-step reduction of metal ions occurs without any external stabilizer or reducer, as plants are all in all candidates in synthesis [18]. Plants possess active biomolecules such as phenols, flavonoids, alkaloids, carboxylic or organic acids, proteins, polysaccharides, and vitamins [19] as well as minerals, which have a tendency to donate electrons to the metal ions, enabling them to form on a nanoscale. Additionally, these active constituents also provide encapsulation on the metal surface besides stabilization [20–22].

*Murraya koenigii*, belonging to the family Rutaceae, is a valuable plant and famous for its aroma [23]. Many medicinal properties are exhibited by the root, leaf, and bark of this plant [24]. The stomachic ailments, such as diarrhea, dysentery, as well as vomiting, can be treated by using its leaves. Similarly, roots and leaves also show anti-inflammatory, analgesic, anti-itching, anticancer, antibacterial, antifungal, and anthelmintic characteristics [25]. In addition, the eruptions and poisonous animals' bites are cured by applying its root and bark externally [26, 27]. These medicinal traits provided a base to use this plant for the synthesis of Au*nps.

The contemporary attempt was made to synthesize Au*nps using the extract of *Murraya koenigii* (EMk) in a single step with an optimization process. The structural elucidation of green-synthesized Au*nps was

executed using UV/Visible spectroscopy, FTIR, TEM, SEM, XRD, and EDX techniques. The characterized Au*nps were screened against selected microbes for antimicrobial traits. The total phenolic and flavonoid content, antioxidant, and hemolytic activity were also assessed. An in vivo biological compatibility study was carried out to determine the bio-efficacy of these nanoparticles.

## Materials and methods

### Chemicals and reagents

Chloroauric ($HAuCl_4$) salt was procured from Sigma Aldrich. Aqua regia, nutrient agar, Mueller Hinton agar (MHA) (Sigma-Aldrich: 70191), chloramphenicol (Sigma-Aldrich: C0378), Mueller Hinton broth (MHB) (Sigma-Aldrich: CM0405B), methanol (Merck Millipore: 106009), 2,2-Diphenyl-1-picrylhydrzyl (DPPH) (Sigma-Aldrich: 257621), sodium carbonate (Merck: 106393), Folin Ciocalteu reagent (FCR) (Merck Millipore: 109001), aluminium chloride (Sigma-Aldrich: 801081), potassium acetate (Merck Millipore: 104820), quercetin (Sigma-Aldrich: Q4951), sodium nitroprusside (Merck Millipore: 106541), phosphate buffer (Merck Millipore: 146592), Griess reagent (Sigma-Aldrich: G4410), gallic acid (Sigma-Aldrich: G7384), vitamin C (Merck Millipore: 47863), butylated hydroxy toluene (BHT) (Merck Millipore: 817074), phosphate buffer saline (PBS) (Sigma-Aldrich: P4244), formalin (Merck Millipore: 104003), paraffin (Sigma-Aldrich: GL4141), hematoxylin (Sigma-Aldrich: H9627), eosin, and de-ionized water were used. All the chemicals and reagents were of analytical grade.

### Plant leaves' collection for EMk preparation

The research work was performed in the Department of Chemistry, University of Agriculture, Faisalabad with latitude (31.4294) and longitude (73.0750) during the summer season and the respective leaves (from matured plant) were collected from the Botanical Garden of the University of Agriculture, Faisalabad during the month of July and got authenticated. After collection, leaves were placed under running tap water for the removal of dust and any debris. The final washing was done with distilled water, following which leaves were dried in the air (under shade) for three days. Finally, the respective leaves were ground with a domestic grinder, and the powder was used to make an extract. The 5 g of powder of these leaves was dissolved in 100 mL de-ionized water, and the mixture was placed in a water bath for 15 minutes at 60°C. After cooling at room temperature, the mixture was filtered with Whatman No. 1 filter paper (pore size: 2.5 µm) for collection of EMk [5, 28].

### Synthesis procedure of Au*nps

The EMk of the volume of 10 mL was added drop wise into 1 mM Au salt solution with constant stirring at room temperature. The variation in solution color was observed and monitored using UV/Visible spectroscopy using de-ionized water as a blank [29]. The precursor and reducing agent were also subject to analysis. After completing the synthesis process, the nanoparticles were centrifuged at 4,000 rpm for 10 minutes with four times repeated washing using de-ionized water. After neutralization, these nanoparticles were freeze dried via lyophilizer for characterization. A complete method of study has been provided in the form of a graphical illustration in Figure 1.

### Kinetic study

The synthesis process was analyzed through the study of variation in values of EMk's volume (1–30 mL), Au salt solution's concentration (1–5 mM), pH (3–9), temperature (30–70°C), and time (5 minutes–24 hours) of reaction. All other parameters were kept constant during the variation of one parameter (EMk: 10 mL, Au salt solution: 1 mM, temperature: 30°C, pH: 7, and time: 24 hours).

### Characterization

The synthesis was confirmed using a double beam UV/Visible spectrophotometer (Perkin Elmer: LAMBDA 365) in the range of 300 nm to 800 nm with regular intervals [30]. The functional groups of EMk and their presence in Au*nps were identified with the help of FTIR spectrophotometer (Perkin Elmer 400: US) with

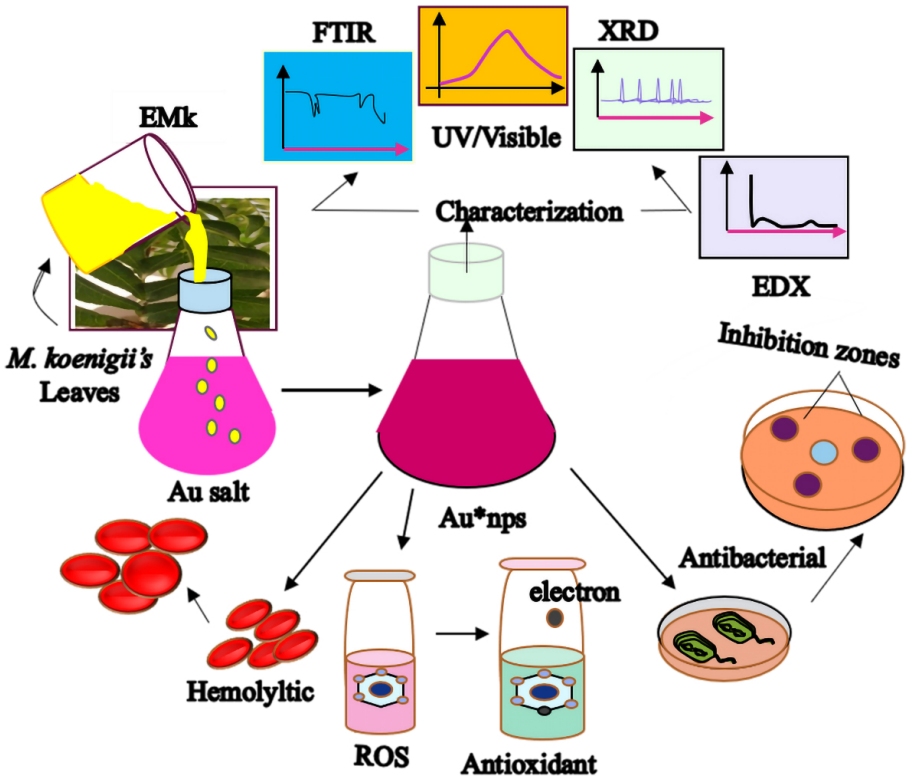


**Figure 1. Graphical view representing synthesis and applications of Au*nps.** Au*nps: gold nanoparticles; EMk: extract of *Murraya koenigii*

transmittance mode setting at 4,000–500 $cm^{-1}$ range [31]. The size and shape of nanoparticles were determined through TEM (Philips CM 10: US). The sample solution was prepared, from which 2 drops were dried on carbon coated grid, and a 200 kV accelerating voltage was applied for image formation [32]. The morphological analysis was done via SEM (Zeiss Evo LS10: Germany) with 25 kV operating voltage by taking approximately 2 drops of nanoparticles solution on carbon coated stub and dried [33]. The X-ray diffractometer (XRD, X'Pert Pro: Netherlands) was employed to determine the crystalline nature of nanoparticles. The diffraction intensities at 20–80° in the 2θ range with 40 kV accelerated voltage and 30 mA current were used. The XRD pattern was analyzed at Cu-Kα radiation with 1.5406 A° wavelength [34]. The elemental character was estimated through EDX (Oxford X-Max 20 WDX: UK) with an operating voltage of 15 keV [35].

## Antibacterial analysis

Antibacterial assessment of Au*nps, EMk, and Au salt was carried out using agar well method against *Escherichia coli* and *Bacillus subtilis* by adopting a protocol used by Rajesh et al. [36] with slight modification. The bacterial strains were procured from the Medicinal Biochemistry Research Lab, University of Agriculture, Faisalabad. The strains were cultured in 2% MHA solution (prepared in de-ionized water) and autoclaved. The solution was dispensed in cleaned, autoclaved Petri plates. After a few minutes (required for gel's solidification), 200 µL of fresh bacterial cultures were poured into plates. The holes were made in the gel with a cork borer, and different concentrations (20, 40, 60, 80, and 100 µg/mL) of samples of the volume of 100 µL were transferred into these holes, where chloramphenicol (standard) was used as a positive control and de-ionized water as negative control. The plates were incubated at 37°C for 24 hours, following which inhibitory zones were measured.

## Phenolic estimation

### Total phenolic content (TPC)

The test solution was prepared using different concentrations (25, 50, 100, 250, 500, and 1,000 µg/mL) of 20 µL of each of Au*nps and EMk solution in de-ionized water and mixed with 90 µL FCR and incubated for

5 minutes at room temperature. Then, the reaction mixture was mixed with 5% sodium carbonate (90 µL) for neutralization and allowed to incubate for another 15 minutes. The incubated solution was transferred into 96-well plate, and results were obtained at 750 nm. Gallic acid was used as a standard, and results were expressed as microgram gallic acid equivalent per milligram [37].

### Total flavonoid content (TFC)

TFC was determined through the colorimetric method of aluminium chloride. The testing solution was prepared by taking different concentrations of Au*nps and EMk (each 20 µL) and mixed with 10 µL aluminium chloride (10%), 10 µL potassium acetate (1 M), and 160 µL distilled water. After mixing, the reaction mixture was incubated for half an hour at room temperature, and reading was taken at 415 nm using a 96-well plate. Quercetin was employed as a standard, and results were represented as micrograms quercetin equivalent per milligram [38].

## Antioxidant activities

### DPPH activity

The antioxidant activity of Au*nps, EMk, and vitamin C (standard) at different concentrations was measured using the DPPH radical scavenging assay with modification from [39]. The test tube solution was prepared by mixing samples with 1 mL methanolic DPPH solution (0.1 mM) and vortexing. The solutions were kept in the dark for 40 minutes, and absorbance was recorded at 517 nm. The de-ionized water was used as a blank. The radical scavenging activity was determined by using Equation 1.

$$\text{Radical inhibition} \quad (\%) \quad = \frac{A_0 - A_x}{A_0} \times 100\% \tag{1}$$

where $A_0$ is Absorbance of control, $A_x$ is absorbance of sample/standard.

### Nitric oxide (NO) activity

The NO radical scavenging activity of Au*nps, EMk, and BHT (standard) at their increased concentrations was determined according to [40] by mixing with 5 mM sodium nitroprusside and phosphate buffer (pH 7.4). The resultants were incubated for 35 minutes at 25°C, followed by mixing with Griess reagent. The absorbance of the solution was measured at 546 nm. The free radical scavenging activity was calculated using Equation 1.

## Hemolytic activity

The compatibility of Au*nps with the biological system was gauged by the release of hemoglobin amount from RBCs after exposure to these nanoparticles. The healthy human blood sample was collected in a sterile Falcon tube and treated with heparin (to avoid clotting) and centrifuged for 15 minutes at 1,000 rpm. After careful removal of supernatant, the pellet was washed with chilled PBS (pH 7.4) at 3,000 rpm for 5 minutes, followed by removing supernatant. This washing process was repeated three times. The washed suspension (180 µL) was mixed with different concentrations (10–100 µg/mL) of Au*nps (20 µL) and incubated for 10 minutes at 37°C. The ice was used to chill the incubated mixtures (5 minutes), and the respective mixture was centrifuged for 5 minutes at 4,200 rpm. Dilution was performed by taking 100 µL of supernatant and 900 µL PBS. The absorbance was recorded at 576 nm, and for this assay, Triton-X-100 (0.1%) was used as a positive and PBS as a negative control. The hemolysis (%) was calculated using Equation 2.

$$\text{Hemolysis}(\%) = \frac{A_{\text{sample}} - A_{\text{PBS}}}{A_{\text{Triton}} - A_{\text{PBS}}} \times 100\% \tag{2}$$

where $A_{\text{sample}}$ is absorbance of sample, $A_{\text{PBS}}$ is absorbance of PBS, $A_{\text{Triton}}$ is absorbance of Triton-X-100.

## Histopathology study

The animal (Wistar rats: 4 to 6 months old) study was performed to evaluate the effect of Au*nps for determining the in vivo biological compatibility. The study was carried out with the permission of the Office

of Research and Commercialization (ORIC), University of Agriculture, Faisalabad, which issued a Bioethics Certificate. The guidelines of ethics regarding the use of animals during the in vivo study were followed according to the Punjab Biosafety Rules, 2014. Animals were divided into two groups: treated (Au*nps) and control (PBS), each consisting of 4 animals, which were weighed before and after the dose period (14 days). The sample of Au*nps (100 µg/mL) was sonicated for 15 minutes and injected to animals by tail vain (treated group) and PBS for control group under similar conditions for alternate days and after completing four doses, the animals were sacrificed for their lives to collect the liver coefficients after applying anesthesia via Pentobarbital sodium injection according to the International Ethical Guidelines in order to avoid excruciation to these animals as much as possible. Subsequently, the respective organs were placed in formalin (10%) and further treatment was performed, including fixation (formalin), sectioning (paraffin), and staining (hematoxylin and eosin) as mentioned by Mumtaz et al. [23]. The images were taken using an optical microscope.

### Statistical analysis

All experimental procedures were repeated five times and articulated as mean ± S.E. One-way ANOVA was employed (Minitab 17.1.0) to make comparisons among tested groups using the "*t*" test, while *p* values less than 0.05, 0.01 were measured as significant.

## Results

### Synthesis

The absorbance profile of Au*nps, along with EMk and Au salt, was represented in Figure 2. The reddish-orange color appeared just after mixing pale color EMk and orange Au salt solution, which provided preliminary evidence of synthesis. After initial visual inspection, the solution was monitored via UV/Visible analysis at regular intervals. With the passage of time, the synthesis progressed as shown by the peak formation.

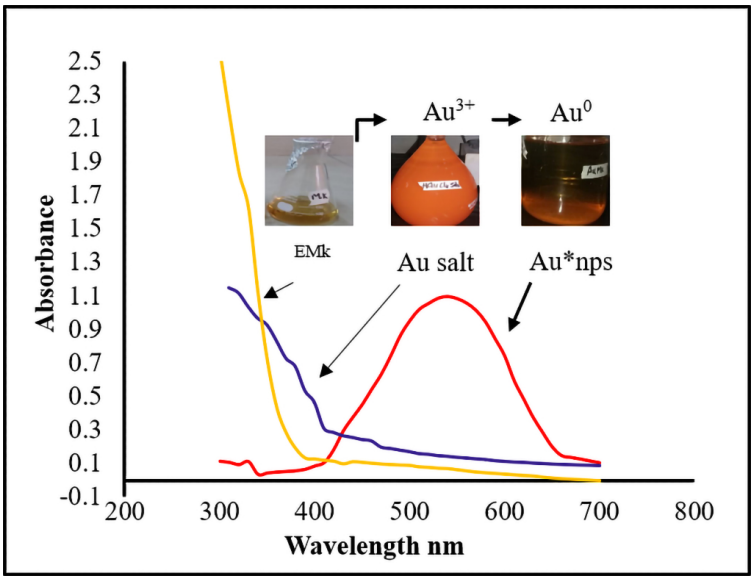


**Figure 2. Synthesis of Au*nps as observed through UV/Visible absorption spectra of Au*nps, Au salt, and EMk as a function of wavelength.** Au*nps: gold nanoparticles; EMk: extract of *Murraya koenigii*

### Kinetic study

The role of reducing agent's volume on the synthesis of Au*nps was evaluated by varying the volume of EMk. The band intensity was gradually enhanced on increasing the volume from 1 mL to 10 mL with a quick synthesis process, as indicated by the spectra in Figure 3A, whereas further increase in volume (from 20 mL to 30 mL) resulted in band widening, which depicted the synthesis of large-sized nanoparticles.

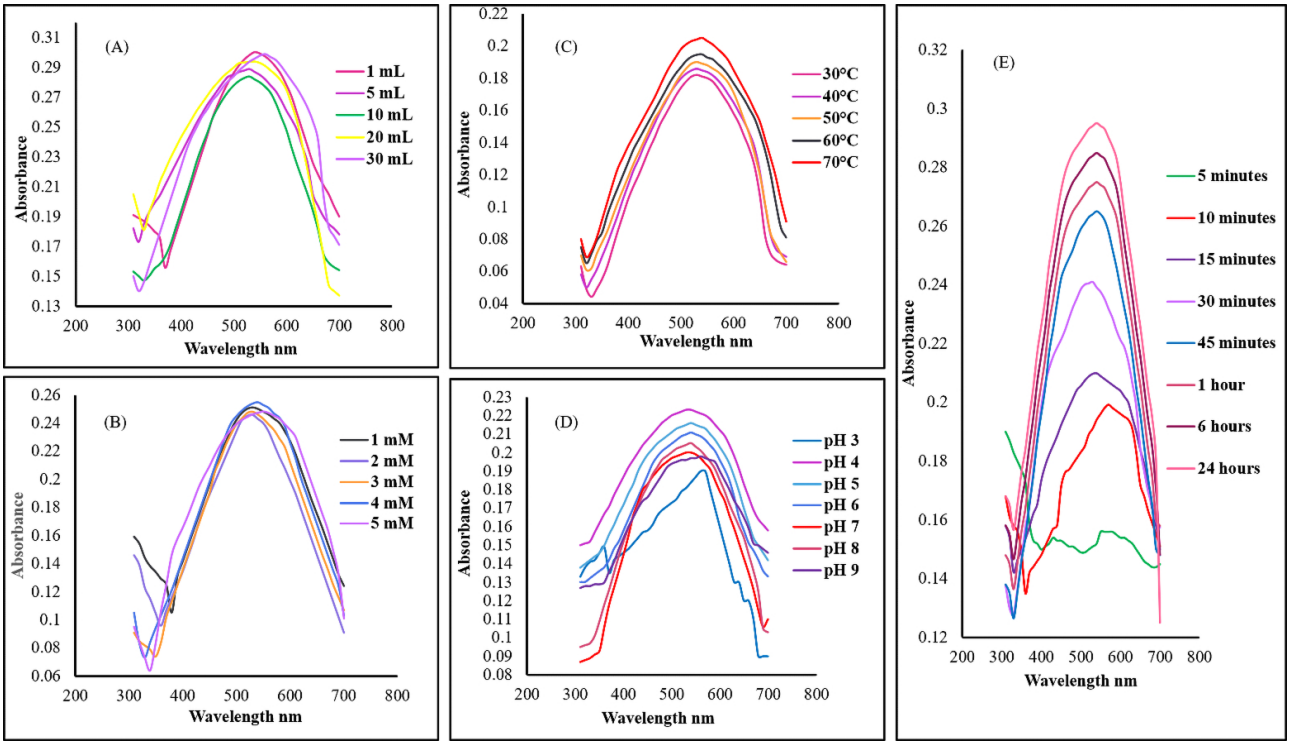


**Figure 3. UV/Visible spectra showing the effect of environmental variables.** (**A**): EMk volume; (**B**): Au salt concentration; (**C**): temperature; (**D**): pH; (**E**): time on synthesis of Au*nps. Au*nps: gold nanoparticles; EMk: extract of *Murraya koenigii*

One of the crucial factors influencing the synthesis process was the precursor's concentration, as shown by the spectra in Figure 3B. The 1–5 mM increase in Au salt concentration resulted in increased band intensity from 530–560 nm.

The study of temperature variation during synthesis appeared to be extremely useful. Initially, at low temperature (30°C), the synthesis rate was slowed with the least band intensity; on the contrary, with the rise in temperature from 40–70°C, significant synthesis and band intensity with absorption band (530–570 nm) were observed as illustrated in Figure 3C. Similarly, an abrupt reduction was observed at high temperature, which indicated synthesis completion within a short time period. However, very high temperature also causes agglomeration in the reaction mixture. Thereby, the optimum temperature was chosen as 60°C.

The effect of pH is considered fundamental to explore the synthesis progress, as the pH study is an important parameter that plays a key role in the synthesis. During analysis, investigation showed that the synthesis was negligible at high acidic value and was fruitful near neutral and in slightly alkaline medium, which can be acknowledged from the spectra in Figure 3D.

The nanoparticles' synthesis requires proper incubation time, which is necessary to investigate as the interaction of the reducing agent with that of the precursor leads to nucleation and crystal growth. Therefore, after mixing, the solution was regularly monitored, indicating synthesis, which was affirmed in the form of a band during different time intervals as shown in Figure 3E.

The optimum conditions of synthesis were selected as: 10 mL (volume of EMk), 1 mM (concentration of Au*nps), 60°C (temperature), 7 (pH), and 24 hours (reaction time). These optimal conditions were used further for performing characterization and biological activities.

## Characterization

### FTIR

The FTIR spectra of EMk are given in Figure 4B. The FTIR spectra of EMk showed different bands or peaks at different positions, such as a broad band at 3,503–2,019 $cm^{-1}$, which might occur due to the phenol functional group or N–H/C–H/O–H stretching bonding of amines, amides, –COOH, or C–N groups. Possibly,

due to C=C stretching, one strong peak was observed at 1,620 $cm^{-1}$, whereas a small peak at 1,769 $cm^{-1}$ could correspond to the carbonyl functional group. Similarly, some other consecutive peaks appeared at 1,481 $cm^{-1}$, 1,308 $cm^{-1}$, 1,182 $cm^{-1}$, and 663 $cm^{-1}$ might be represented by the aliphatic ether among some other functional groups. Herein, clear shifting of peaks was observed when comparing the spectra of Au*nps with EMk, as in Figures 4A, B.

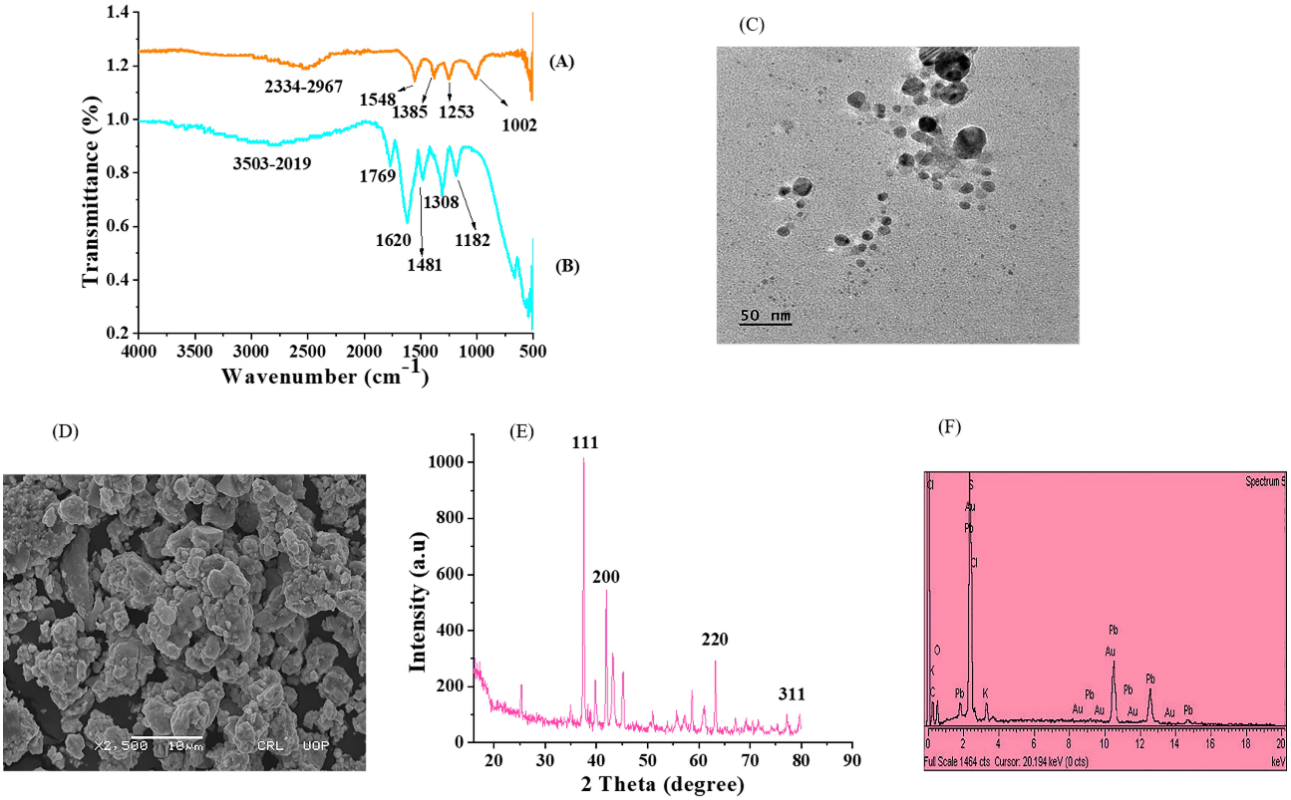


**Figure 4. Characterization.** FTIR spectra of (**A**) Au*nps and (**B**) EMk; (**C**): TEM micrographs; (**D**): SEM; micrographs; (**E**): XRD pattern; and (**F**): EDX spectra of Au*nps

The rearrangement of functional groups was observed in the spectra of Au*nps in Figure 4A. Due to C–H stretching (aldehyde) or S–H thiol group, a band might emerge at 2,334–2,967 $cm^{-1}$. At 1,548 $cm^{-1}$, 1,385 $cm^{-1}$, and 1,002 $cm^{-1}$, consecutive peaks were located, which might be due to the presence of the nitro group, C–H bending (alkane), and C–O stretching of aromatic ester, respectively. The slight transfer of peak from the origin of EMk in Au*nps indicated the flourishing reduction of $Au^{3+}$ to $Au^{0}$ during the synthesis process.

## TEM

The size information is vital to identify the proper biological efficiency of synthesized nanoparticles. For this, the TEM analysis has been carried out, which revealed that the biosynthesized Au*nps had 50 nm size and spherical shape as indicated in Figure 4C.

## SEM

The surface morphology can also be explained through the SEM study. The SEM micrographs displayed the spherical shape of Au*nps with some aggregate formation, as shown in Figure 4D.

## XRD

Figure 4E shows the XRD graphical illustration of Au*nps, which indicates the presence of a sharp signal of gold metal, confirming the crystalline nature of nanoparticles.

The diffraction of peaks occurs due to the striking of X-rays with the surface of the metal at a specific angle and direction. The different diffraction peaks at specific index planes, such as 24.65° (111), 34.65° (200), 65.45° (220), and 77.56° (311), had been analyzed in the XRD pattern of Au*nps. These planes clearly showed the crystalline structure of biosynthesized Au*nps. Besides, some minor peaks also arose, which evidenced the presence and encapsulation of bioactive components of EMk on the surface of metal.

### EDX

The EDX analysis confirmed the elemental nature of green synthesized Au*nps as shown in Figure 4F. In addition, some other components such as C, K, Cl, O, and Pb were also observed in trace amounts in the graph.

## Antibacterial activity

The Au*nps exhibited significant antibacterial activity against both bacterial strains at increased concentration. The inhibition zones were considerably higher after applying these nanoparticles. The gram-positive bacterial strain had emerged to be more sensitive toward Au*nps than gram-negative bacteria. The Au*nps inhibited 13 mm and 15 mm growth of *E. coli* and *B. subtilis* strains at 100 µg/mL, as given in Figure 5A. However, under similar circumstances, the standard showed 18 mm and 19 mm growth inhibition against these strains. The incredible potential of Au*nps as an antibacterial agent has been found to be concentration-dependent. The ability of EMk and Au salt to inhibit the growth of these bacterial strains was also increased at increased concentrations.

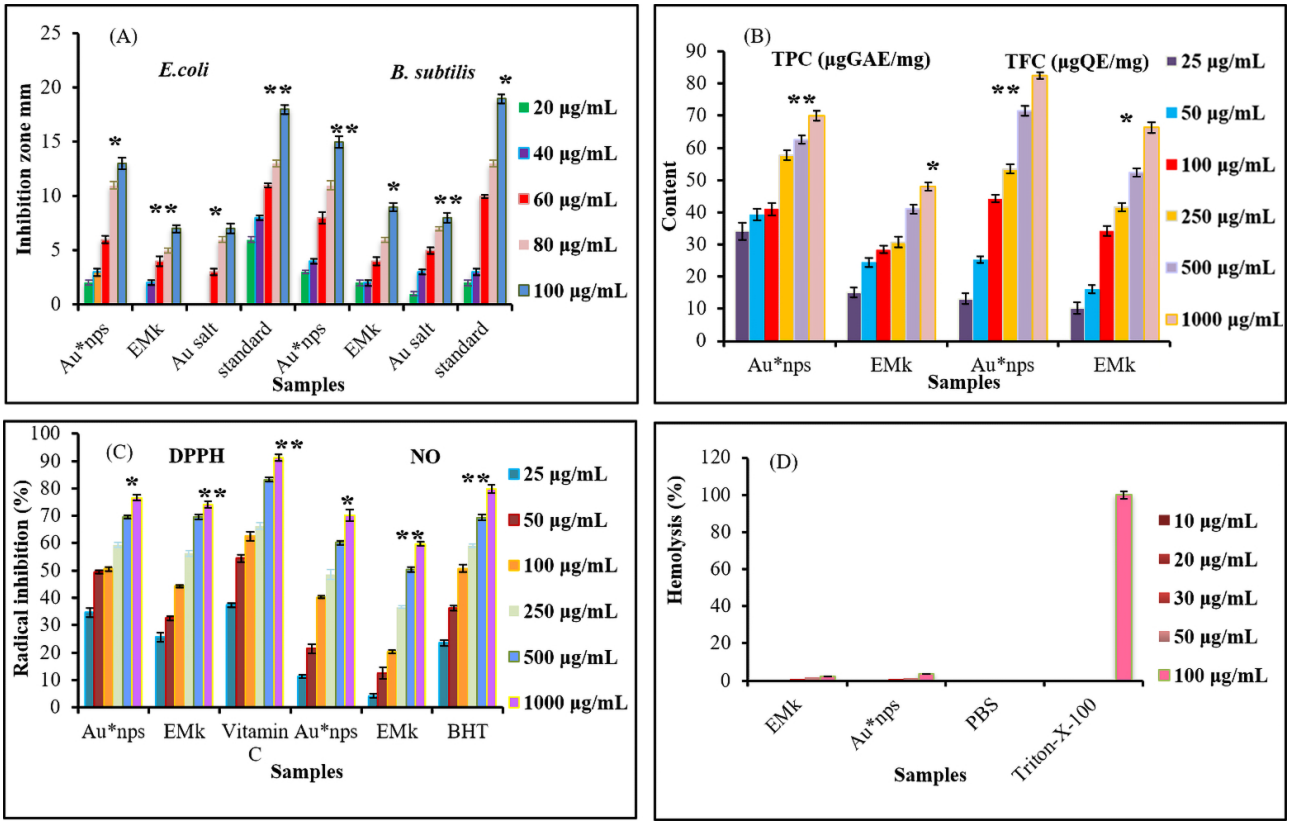


**Figure 5. Au*nps, EMk, and Au salt at different concentrations representing biological activities.** (**A**): Antibacterial against *Escherichia coli* and *Bacillus subtilis*; (**B**): total phenolic; (**C**): antioxidant (DPPH and NO); (**D**): hemolytic. Each value indicates the mean ± S.E. ($n$ = 5), whereas levels of significance are compared Au*nps with EMk, Au salt, and standard. Values were found significant at $p^* < 0.05$, $p^{**} < 0.01$

### Phenolic content

#### TPC and TFC

The TPC study revealed that green-synthesized Au*nps had more TP content (70.92 µg GAE/mg) as compared to EMk (47.03 µg GAE/mg) under similar conditions, as shown by Figure 5B. Similarly, TFC was found to be high in Au*nps (82.66 µg QE/mg) relatively to the extract (66.54 µg QE/mg) as represented in Figure 5B.

### Antioxidant potential

#### DPPH

Figure 5C showed a significant increase in DPPH radical scavenging activity of Au*nps with the rise of concentration of synthesized Au*nps. Evidently, the radical scavenging potential of Au*nps ranged from 34.52% to 76.54% with the increasing concentration from 25 µg/mL to 1,000 µg/mL. Likewise, EMk also showed conspicuous radical quenching ability at increased concentration (25.32–74.34%). However, the standard indicated the significant DPPH scavenging ability (91.21%) compared to Au*nps.

#### NO scavenging potential

Similar to DPPH activity, green synthesized Au*nps equally possessed considerable NO scavenging activity at their increased concentrations (70.65% at 1,000 µg/mL) as shown in Figure 5C. Apart from Au*nps, EMk also demonstrated substantial ability to scavenge peroxynitrite complex species. On the contrary, the reference value was found to be more at 1,000 µg/mL.

### Hemolytic activity

The hemolytic activity of Au*nps with different concentrations (10–100 µg/mL) was evaluated, and the results are given in Figure 5D. The analysis revealed that applied nanoparticles showed minute hemolysis (0.04–3.37%) against RBCs even at increased concentration (10–100 µg/mL). On the other hand, the lysis exhibited by EMk was less than that of the Au*nps. The 0% lysis was observed by PBS, whereas 100% lysis was shown by Triton-X-100.

### Histopathology

The study of histopathology was crucial to conduct in order to examine the behavior of Au*nps within the biological entities. The Au*nps were injected into the animal's body for period of 14 days, and liver tissues were taken and examined via light microscope at 40× (Figure 6), showing no pathological injury or lesion in the liver tissues. This, in turn, indicated the non-toxic effect of applied nanoparticles.

## Discussion

### Synthesis of Au*nps

The synthesis process resulted in the nanosized gold particles. The change in solution color occurs through the phenomenon of surface plasmon resonance (SPR), which, in turn, is associated with the reduction of metal ions to elemental form. Actually, the metal possesses free conduction electrons, which get excited during the SPR phenomenon. Mainly, an electric field is created due to this excitation, which causes oscillation in the electrons responsible for the resonance at a particular wavelength [41]. In our analysis, the strong SPR band was observed around 540 nm, indicating the flourished synthesis process of Au*nps, which is in accordance with the findings performed by [42, 43], whereas no peak formation was observed in the case of Au salt solution or EMk alone.

### Study of environmental variables

Amazingly, the UV/Visible spectral profile is helpful in determining the size and shape of nanoparticles as the presence of single or multiple bands shows the shape and distribution of synthesized nanoparticles. Markedly, the single band represents a homogeneous spherical shape of nanoparticles; whereas, anisotropic character is shown by multiple peak formation.

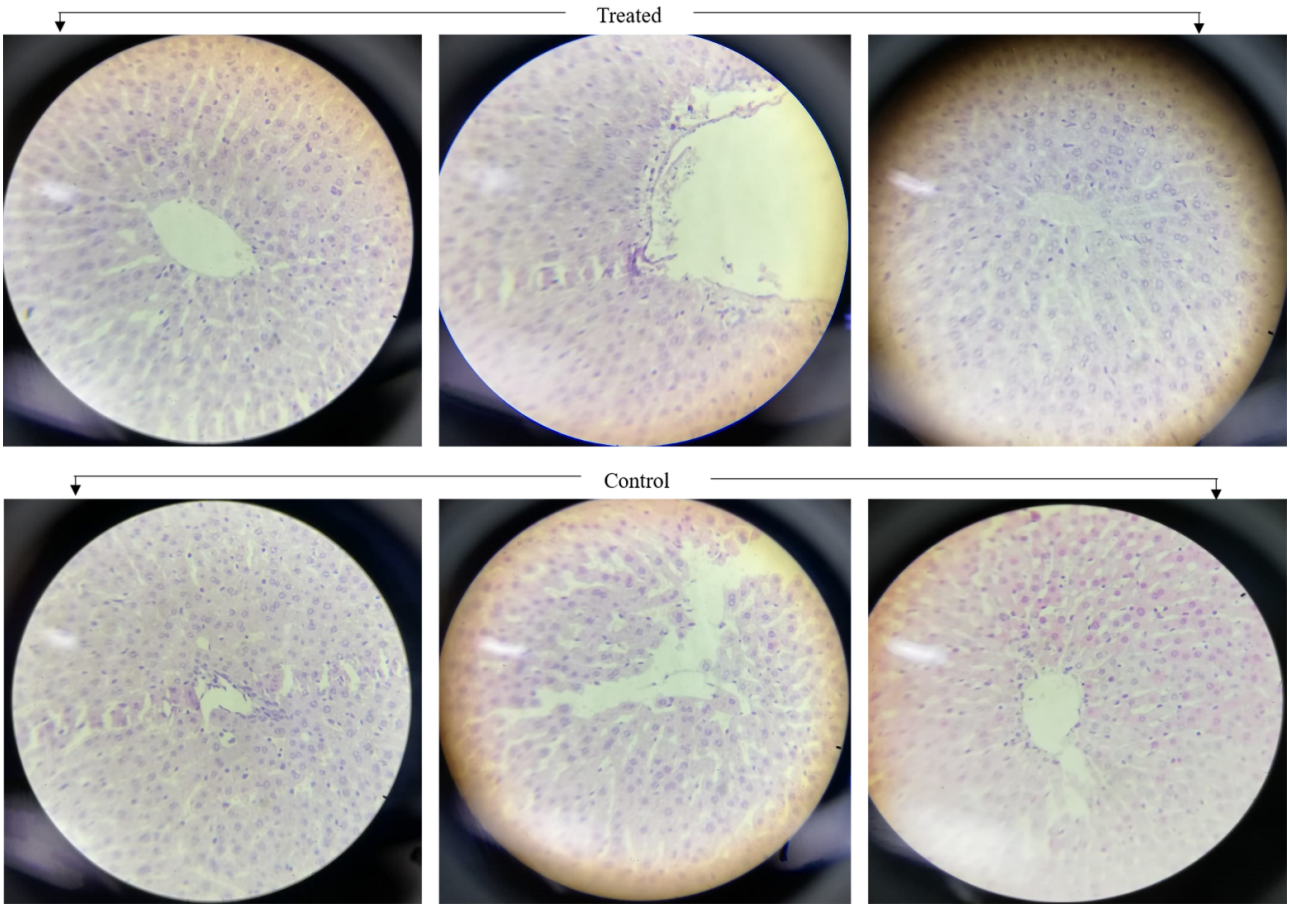


**Figure 6. Histopathological images of liver tissues of Wistar rats exposed to Au*nps (treated) and PBS (control) for 14 days' period (at 40×)**

The significance of volume can be easily clarified with the variation of the SPR band, as it is described in previous reports that the morphology of synthesized nanoparticles is strongly affected by the volume of extract [44]; thus, it correlates with our findings.

The band shifting is fairly obvious from blue to red with a rise in salt concentration representing the particle size change from small to large. Numerous investigations reported that a steadily increased concentration of Au salt solution in the reaction mixture tends to produce aggregates, causing particle size enhancement [45]. In our analysis, the optimum concentration for the reaction synthesis is considered to be 3 mM; nevertheless, the progressive synthesis of Au*nps was observed at 1 mM concentration, forming a narrow SPR band at 560 nm.

Several reports have been confirmed [46, 47] that an increase in temperature favors the synthesis process, as indicated by our findings.

The increased acidic and basic media decreased the synthesis, as the absorption data have been illustrated by blue to red shifts in wavelength with broader bands. Despite the fact that the ionization of basic functional groups boosts the synthesis, having said that, their increased concentration led to precipitation. Therefore, the optimum pH value for the successful synthesis was selected as neutral as prescribed by Mosaviniya and coworkers [48].

Furthermore, the band intensity appeared to increase with time, which proved the successful reduction of gold ions into metallic form after taking up electrons from the reducing agent's functional groups. Eventually, the synthesis took 24 hours for complete reduction, as a further increase in time caused no change in band intensity. Ramesh et al. [17] observed similar results in their work, which thus assisted our findings.

## Characterization

FTIR analysis was considered to be vital for understanding the synthesis of nanoparticles owing to the role of functional groups of EMk and their involvement in reduction. The FTIR data interpreted the fundamental character of various functional groups of EMk for the synthesis of Au*nps; hence, clearly expounded that these functional moieties had a factual place in the reduction process. It is important to discuss that the affinity between the metal of the reducing agent's bioactive components is too strong to enable the new bond formation. Our findings are quite supported by research work described by Khan and colleagues [49], who worked on the synthesis of copper oxide nanoparticles via plant extract and described the role of functional groups during synthesis. Similar to Khan et al. [49], Rabeea et al. [50] reported parallel observations while working on the synthesis of Au*nps.

In fact, the stability of nanoparticles is associated with the bioactive constituents, as no additional or external stabilizer was added in the reaction.

It has been reported by Wahid Wahab et al. [51] that the shape of synthesized nanoparticles is strongly influenced by the nucleation and growth phenomenon during synthesis, as nuclei formation occurs first, followed by crystal growth, which generates different shapes such as spherical, triangular, pentagonal, or hexagonal.

The reason behind the formation of the aggregation of nanoparticles lies in the fact that EMk has various potent functional groups, as indicated from the FTIR spectra, which not only provide electrons to the metal but also give stability by encapsulation on the surface of the metal in the form of a covering sheath. Our results are quite similar to those mentioned by Thanh and colleagues [52] in their work.

The analysis of XRD peaks was compared with pure crystalline gold by using JCPD. Similar investigations were performed by Ansari et al. [53] when investigating silver nanoparticles and Nirmala and coworkers [54] while characterizing synthesized Au*nps from plant extracts.

The presence of other elements in the EDX image confirmed the presence of functional bioactive constituents of EMk and their essential role during synthesis.

The characterization via these analytical techniques provided a basic understanding, which was quite necessary for the interpretation of surface and structural properties of Au*nps.

## Antibacterial activity

The size of nanoparticles has a significant inhibitory effect on the bacterial cell, as the small-sized nanoparticles have the ability to enter the cell [5]. Moreover, the bacterial structure is another important feature that makes them susceptible to the attack of nanoparticles. In this regard, different mechanisms have been proposed to explain the action of metal nanoparticles against bacteria [55]. It is assumed that bacterial cell when exposed to metal nanoparticles, protein replication, hindrance of DNA base, reactive oxygen species' generation, or ribosomal destabilization might occur, which ultimately induces damage to the cell [56]. Another hypothesis states that the enzyme activity of the bacterial cell is probably inhibited when it comes into contact with nanoparticle exposure (Figure 7). *Murraya koenigii* possesses several bioactive components such as carbazole alkaloids (namely mahanimbine, mahanine, and murrayanol) as revealed in several reports [57], which have a strong bactericidal effect as well as studied earlier by Franyoto and coworkers [26]. Together, these bioactive moieties, along with the nanoparticles of metal, can be enough to damage the bacterial cell.

## Phenolic content

The variation in the phenolic content might arise due to the diverse phytochemicals which are present in the plant extracts, such as phenolic, alkaloids, alcoholic, carboxylic, saturated, and unsaturated functional moieties, as investigated by Nagappan et al. [58], due to which they actively participate in the synthesis and reduction of metal ions. The obtained results indicate the biochemical characteristics of nano-capsulated nanoparticles synthesized in a perfect manner, as they modulate specific traits during the synthesis process, which were also investigated by Abdel-Aziz et al. [59] in their studies.

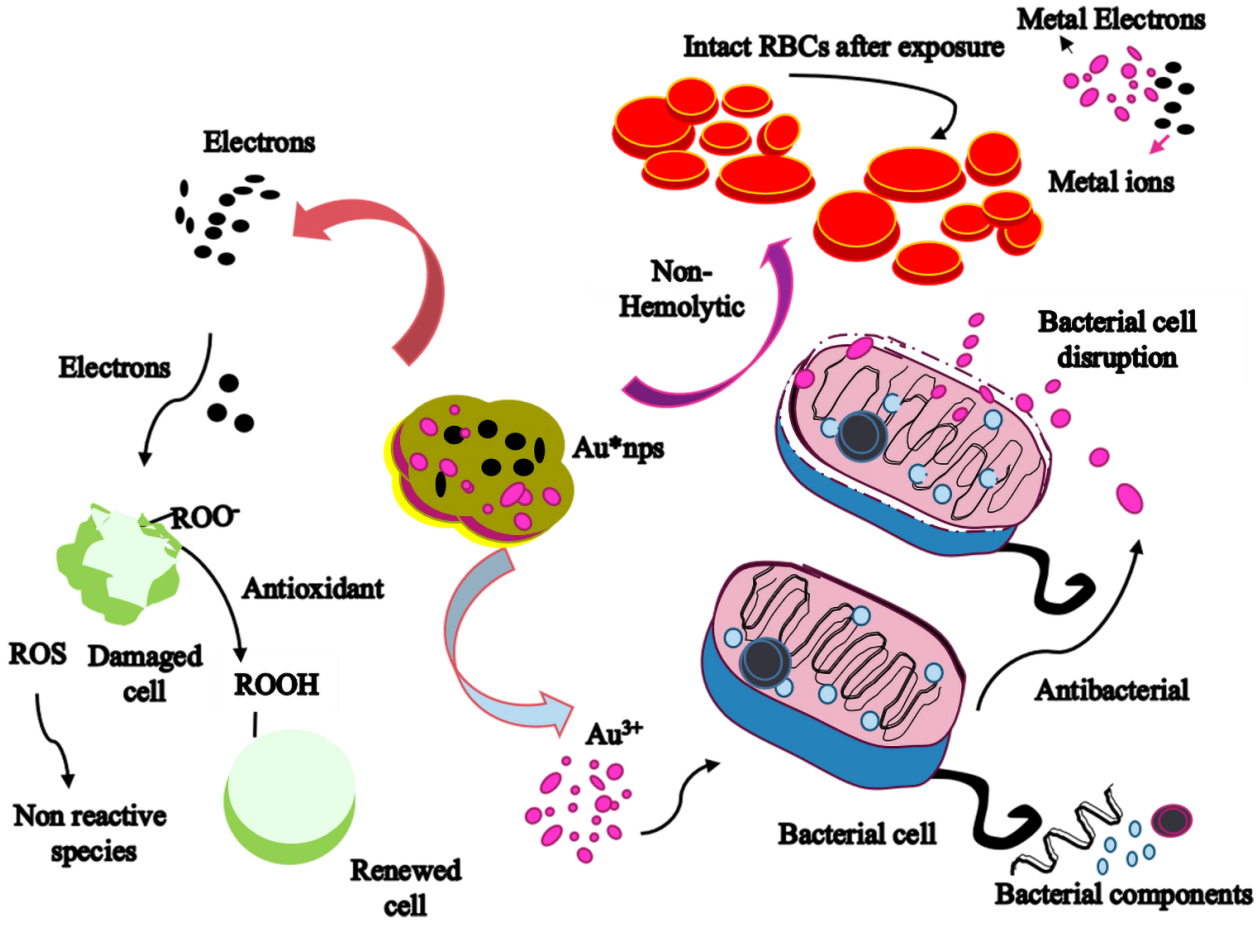


**Figure 7. Mechanism of antibacterial, antioxidant, and hemolytic action of biologically reduced Au*nps against microbial species, ROS, and biocompatibility against RBCs**

A general mechanism of biological properties exhibited by Au*nps has been represented in Figure 7.

## Antioxidant activity

Antioxidant agents have the ability to donate electrons or hydrogen atoms to the stable free radicals, which in turn accept them and convert themselves into nonreactive (stable) form, as in the case of DPPH radical to the nonradical form of DPPH-H [60]. On account of their nature, the biologically reduced Au*nps have prominent radical quenching potential (Figure 7) and represented a good comparison to vitamin C. Apparently, this strong antioxidation capacity possessed by Au*nps facilitates their way to be used in biomedical formulations as reported by Anbukkarasi et al. [61] in similar work when analyzing DPPH scavenging potential of plant mediated silver nanoparticles.

It has been studied that numerous biological functions are accomplished through the NO cycle, such as muscle relaxation, antitumor behavior, antibacterial trait, antifungal potential, blood flow regularization, as well as neuron transmission [41]. Nevertheless, when it reacts with superoxide, it forms peroxynitrite ions, causing oxidative damage, most prominently, DNA fragmentation [42]. Therefore, it is quite necessary to control and regulate the reactions associated with NO. That is why, NO scavenging potential possessed by Au*nps seemed to be excellent, which showed their biomedical behavior. Numerous studies on the *Murraya koenigii* plant have been performed to evaluate its phytochemical constituents, and one similar evaluation was carried out by Balakrishnan and colleagues [62], which evidenced the presence of versatile phytochemicals such as murrayastine, koenidine, cyclomahanimbine, and others, which have tremendous antioxidant potential and easily give electrons to make them (free radicals and other ROS) stable [63]. This ability even enhances in the nanoparticles that are synthesized from them.

### Hemolytic activity

The effect of Au*nps on RBCs needs to be investigated for implementation in biological applications. The least level of toxicity by the nanoparticles on RBCs is an important feature that is fairly crucial to examine for evaluating particular medicinal properties. In fact, the nontoxic behavior of green-synthesized Au*nps emerges due to the presence of surface encapsulation on the metal core, which was provided by functional groups of EMk (Figure 7). Conceivably, the antiradical efficiency of the plasma membrane might be enhanced due to these active biomolecules cause hindrance in the oxidation of biological membranes, ultimately enabling them to be less susceptible to invaders' attack [64].

### Histopathology

The toxicity evaluation is one major aspect to be considered for biomedical purposes, especially for the designation of drugs required for a particular role. Our study proved that these nanoparticles are quite safe for the biological system, as previously explained by Mumtaz et al. [23] and Mukherjee et al. [65] in their work based on the synthesis of silver nanoparticles. Besides, it must be kept in mind that the selected dose was 50 µg/mL, which can be studied further by increasing the concentration so that the exact toxicity and optimum level can be determined.

### Conclusions

Herein, an eco-friendly biological pathway was followed to achieve Au*nps by utilizing EMk via a single step. At first, an absorption band around 540 nm confirmed the prosperous synthesis process. Then, the size and shape of Au*nps were controlled by optimizing the environmental variables, and the whole synthesis was monitored using UV/Visible spectroscopy. Further ahead, the characterization studies had shown a 20–50 nm size of these nanoparticles, spherical shape with some aggregates, crystalline nature as well as elemental form through TEM, SEM, XRD, and EDX analysis, respectively. In addition, the functional moieties were screened using an FTIR study, which evidenced the sole role of EMk in the synthesis of Au*nps. Subsequently, the remarkable biological attributes of the nanoparticles were visualized through phenolic compounds, antioxidant, antibacterial, and hemolytic assays. Final examination of these Au*nps was carried out on Wistar rats, which demonstrated nontoxic effects on liver tissues, proving their biological efficacy, permitting them to be employed as a potential substitute in nano-formulations for curative actions.

## Abbreviations

Au*nps: gold nanoparticles

BHT: butylated hydroxy toluene

DPPH: 2,2-Diphenyl-1-picrylhydrzyl

EMk: extract of Murraya koenigii

FCR: Folin Ciocalteu reagent

MHA: Mueller Hinton agar

NO: nitric oxide

PBS: phosphate buffer saline

TFC: total flavonoid content

TPC: total phenolic content

XRD: X-ray diffractometer

## Declarations

### Author contributions

SM: Conceptualization, Methodology, Investigation, Writing—original draft, Writing—review & editing. IH: Software, Validation, Formal analysis. MJI: Data Curation, Visualization, Supervision. All authors read and approved the submitted version.

### Conflicts of interest

The authors declare that they have no conflicts of interest.

### Ethical approval

The National Biosafety Committee (NBC) from the Office of Research and Commercialization (ORIC), University of Agriculture, Faisalabad, issued the Bioethics Certificate (No. 1321). The guidelines of ethics regarding the usage of animals during the in vivo study were adopted according to the Punjab Biosafety Rules, 2014.

### Consent to participate

Not applicable.

### Consent to publication

Not applicable.

### Availability of data and materials

Any relevant data will be made available on request.

### Funding

Not applicable.



## Publisher's note



## References

1. Ahmad T, Bustam MA, Irfan M, Moniruzzaman M, Anwaar Asghar HM, Bhattacharjee S. Green synthesis of stabilized spherical shaped gold nanoparticles using novel aqueous Elaeis guineensis (oil palm) leaves extract. J Mol Struct. 2018;1159:167–73. [DOI]
2. Dhayalan M, Denison MIJ, Ayyar M, Gandhi N, Krishnan K, Abdulhadi B. Biogenic synthesis, characterization of gold and silver nanoparticles from Coleus forskohlii and their clinical importance. J Photochem Photobiol B. 2018;183:251–7. [DOI] [PubMed]
3. Zarzuela R, Luna MJ, Gil MLA, Ortega MJ, Palacios-Santander JM, Naranjo-Rodríguez I, et al. Analytical determination of the reducing and stabilization agents present in different Zostera noltii extracts used for the biosynthesis of gold nanoparticles. J Photochem Photobiol B. 2018;179:32–8.
4. Parnianchi F, Nazari M, Maleki J, Mohebi M. Combination of graphene and graphene oxide with metal and metal oxide nanoparticles in fabrication of electrochemical enzymatic biosensors. Int Nano Lett. 2018;8:229–39. [DOI]

5. Mumtaz S, Nadeem R, Sarfraz RA, Shahid M. Mechanism Study of Green Synthesis and Antibacterial Attribute of *Polyalthia longifolia* Based Gold Nanoparticles. J Nano Res. 2022;75:1–16. [DOI]
6. Ahmad AS, Sachi Das S, Khatoon A, Tahir Ansari M, Afzal M, Saquib Hasnain M, et al. Bactericidal activity of silver nanoparticles: A mechanistic review. Mater Sci Energy Tech. 2020;3:756–69. [DOI]
7. Sargazi S, Laraib U, Er S, Rahdar A, Hassanisaadi M, Zafar MN, et al. Application of Green Gold Nanoparticles in Cancer Therapy and Diagnosis. Nanomaterials (Basel). 2022;12:1102. [DOI] [PubMed] [PMC]
8. Mumtaz S, Khattak S, Rehman FU, Muhammad P, Hanif S. Bionanocomposites as a new platform for drug delivery systems. In: Das S, Thomas S, Das PP, editors. Novel Platforms Drug Delivery Applications. Woodhead Publishing; 2023. pp. 289–315. [DOI]
9. Murali M, Mahendra C, Nagabhushan, Rajashekar N, Sudarshana M, Raveesha K, et al. Antibacterial and antioxidant properties of biosynthesized zinc oxide nanoparticles from *Ceropegia candelabrum* L. - An endemic species. Spectrochim Acta A Mol Biomol Spectrosc. 2017;179:104–9. [DOI] [PubMed]
10. Al-Sheddi ES, Farshori NN, Al-Oqail MM, Al-Massarani SM, Saquib Q, Wahab R, et al. Anticancer Potential of Green Synthesized Silver Nanoparticles Using Extract of Nepeta deflersiana against Human Cervical Cancer Cells (HeLA). Bioinorg Chem Appl. 2018;2018:9390784. [DOI] [PubMed] [PMC]
11. Şahin B, Aygün A, Gündüz H, Şahin K, Demir E, Akocak S, et al. Cytotoxic effects of platinum nanoparticles obtained from pomegranate extract by the green synthesis method on the MCF-7 cell line. Colloids Surf B Biointerfaces. 2018;163:119–24. [DOI] [PubMed]
12. Shah JH, Fiaz M, Athar M, Ali J, Rubab M, Mehmood R, et al. Facile synthesis of N/B double-doped $Mn_2O_3$ and $WO_3$ nanoparticles for dye degradation under visible light. Environ Technol. 2019;41:2372–81. [DOI]
13. Ali J, Ali N, Wang L, Waseem H, Pan G. Revisiting the mechanistic pathways for bacterial mediated synthesis of noble metal nanoparticles. J Microbiol Methods. 2019;159:18–25. [DOI] [PubMed]
14. Pantidos N, Edmundson MC, Horsfall L. Room temperature bioproduction, isolation and anti-microbial properties of stable elemental copper nanoparticles. N Biotechnol. 2018;40:275–81. [DOI] [PubMed] [PMC]
15. Naraginti S, Li Y. Preliminary investigation of catalytic, antioxidant, anticancer and bactericidal activity of green synthesized silver and gold nanoparticles using Actinidia deliciosa. J Photochem Photobiol B. 2017;170:225–34. [DOI] [PubMed]
16. Saha J, Begum A, Mukherjee A, Kumar S. A novel green synthesis of silver nanoparticles and their catalytic action in reduction of Methylene Blue dye. Sustain Environ Res. 2017;27:245–50. [DOI]
17. Ramesh A, Devi DR, Battu G, Basavaiah K. A Facile plant mediated synthesis of silver nanoparticles using an aqueous leaf extract of *Ficus hispida* Linn. f. for catalytic, antioxidant and antibacterial applications. S Afr J Chem Eng. 2018;26:25–34. [DOI]
18. Baruah D, Goswami M, Yadav RNS, Yadav A, Das AM. Biogenic synthesis of gold nanoparticles and their application in photocatalytic degradation of toxic dyes. J Photochem Photobiol B. 2018;186:51–8. [DOI] [PubMed]
19. Catarino MD, Silva AMS, Cardoso SM. Phycochemical Constituents and Biological Activities of *Fucus* spp. Mar Drugs. 2018;16:249. [DOI] [PubMed] [PMC]
20. Francis S, Joseph S, Koshy EP, Mathew B. Green synthesis and characterization of gold and silver nanoparticles using Mussaenda glabrata leaf extract and their environmental applications to dye degradation. Environ Sci Pollut Res Int. 2017;24:17347–57. [DOI] [PubMed]
21. Abdel-Raouf N, Al-Enazi NM, Ibraheem IB. Green biosynthesis of gold nanoparticles using Galaxaura elongata and characterization of their antibacterial activity. Arabian J Chem. 2017;10:S3029–39. [DOI]
22. Mata R, Bhaskaran A, Sadras SR. Green-synthesized gold nanoparticles from *Plumeria alba* flower extract to augment catalytic degradation of organic dyes and inhibit bacterial growth. Particuology. 2016;24:78–86. [DOI]

23. Mumtaz S, Nadeem R, Sarfraz RA, Shahid M. Medicinal aspects of Murraya koenigii mediated silver nanoparticles. Adv Nano Res. 2021;11:657–65. [DOI]
24. Punuru P, Sujatha D, Kumari B, Charisma VVL. Evaluation of aqueous extract of Murraya koenigii in unilateral renal ischemia reperfusion injury in rats. Indian J Pharmacol. 2014;46:171–5. [DOI] [PubMed] [PMC]
25. Selamoglu Z. Polyphenolic Compounds in Human Health with Pharmacological Properties. J Tradi Med Clin Natur. 2017;6:e138. [DOI]
26. Franyoto YD, Nurrochmad A, Fakhrudin N. *Murraya koenigii* L. Spreng.: An updated review of chemical composition, pharmacological effects, and toxicity studies. J Appl Pharm Sci. 2024;14: 011–27. [DOI]
27. Tahia F, Sikder MAA, Sayeed MA, Rashid MA. Bioactivities of Murraya koenigii (Linn.) and Adina cordifolia (Roxb.). Bangla Pharma J. 2015;18:25–9. [DOI]
28. Dong C, Cao C, Zhang X, Zhan Y, Wang X, Yang X, et al. Wolfberry fruit (Lycium barbarum) extract mediated novel route for the green synthesis of silver nanoparticles. Optik. 2017;130:162–70. [DOI]
29. Mythili R, Selvankumar T, Srinivasan P, Sengottaiyan A, Sabastinraj J, Ameen F, et al. Biogenic synthesis, characterization and antibacterial activity of gold nanoparticles synthesized from vegetable waste. J Mol Liq. 2018;262:318–21. [DOI]
30. Aygun A, Ozdemir S, Gulcan M, Cellat K, Sen F. Synthesis and Characterization of Reishi Mushroom-mediated Green Synthesis of Silver Nanoparticles for the Biochemical Applications. J Pharm Biomed Anal. 2020;178:112970. [DOI] [PubMed]
31. Thakur B, Kumar A, Kumar D. Green synthesis of titanium dioxide nanoparticles using Azadirachta indica leaf extract and evaluation of their antibacterial activity. S Afr J Bot. 2019;124:223–7. [DOI]
32. Aadil KR, Pandey N, Mussatto SI, Jhad H. Green synthesis of silver nanoparticles using acacia lignin, their cytotoxicity, catalytic, metal ion sensing capability and antibacterial activity. J Envir Chem Eng. 2019;7:103296. [DOI]
33. Arya A, Mishra V, Chundawat TS. Green synthesis of silver nanoparticles from green algae (*Botryococcus braunii*) and its catalytic behavior for the synthesis of benzimidazoles. Chem Data Collect. 2019;20:100190. [DOI]
34. Nagalingam M, Kalpana VN, Rajeshwari VD, Panneerselvam A. Biosynthesis, characterization, and evaluation of bioactivities of leaf extract-mediated biocompatible gold nanoparticles from *Alternanthera bettzickiana*. Biotechnol Rep (Amst). 2018;19:e00268. [DOI] [PubMed] [PMC]
35. Fatima R, Priya M, Indurthi L, Radhakrishnan V, Sudhakaran R. Biosynthesis of silver nanoparticles using red algae Portieria hornemannii and its antibacterial activity against fish pathogens. Microb Pathog. 2020;138:103780. [DOI] [PubMed]
36. Rajesh K, Ajitha B, Reddy YAK, Suneetha Y, Reddy PS. Assisted green synthesis of copper nanoparticles using Syzygium aromaticum bud extract: Physical, optical and antimicrobial properties. Optik. 2018; 154:593–600. [DOI]
37. Singh C, Kumar J, Kumar P, Chauhan BS, Tiwari KN, Mishra SK, et al. Green synthesis of silver nanoparticles using aqueous leaf extract of *Premna integrifolia* (L.) rich in polyphenols and evaluation of their antioxidant, antibacterial and cytotoxic activity. Biotechnol Biotechnol Equip. 2019;33: 359–71. [DOI]
38. Phull AR, Abbas Q, Ali A, Raza H, Kim SJ, Zia M, et al. Antioxidant, cytotoxic and antimicrobial activities of green synthesized silver nanoparticles from crude extract of *Bergenia ciliata*. Future J Pharm Sci. 2016;2:31–6. [DOI]
39. Dauthal P, Mukhopadhyay M. Antioxidant activity of phytosynthesized biomatrix-loaded noble metallic nanoparticles. Chin J Chem Eng. 2018;26:1200–8. [DOI]
40. Rajan A, Rajan AR, Philip D. *Elettaria cardamomum* seed mediated rapid synthesis of gold nanoparticles and its biological activities. OpenNano. 2017;2:1–8. [DOI]

41. Manikandakrishnan M, Palanisamy S, Vinosha M, Kalanjiaraja B, Mohandoss S, Manikandan R, et al. Facile green route synthesis of gold nanoparticles using *Caulerpa racemosa* for biomedical applications. J Drug Delivery Sci Tech. 2019;10:101345. [DOI]
42. Mumtaz S, Nadeem R, Sarfraz RA, Shahid M. Synthesis, Characterization, and Evaluation of Antimicrobial and Antioxidant Potential of *Polyalthia longifolia* Mediated Copper Nanoparticles. J Nano Res. 2021;68:35–51. [DOI]
43. Medhe S, Bansal P, Srivastava MM. Enhanced antioxidant activity of gold nanoparticle embedded 3,6-dihydroxyflavone: a combinational study. Appl Nanosci. 2012;4:153–61. [DOI]
44. Kang F, Qu X, Alvarez PJJ, Zhu D. Extracellular Saccharide-Mediated Reduction of $Au^{3+}$ to Gold Nanoparticles: New Insights for Heavy Metals Biomineralization on Microbial Surfaces. Environ Sci Technol. 2017;51:2776–85. [DOI] [PubMed]
45. Ma L, Su W, Liu J, Zeng X, Huang Z, Li W, et al. Optimization for extracellular biosynthesis of silver nanoparticles by Penicillium aculeatum Su1 and their antimicrobial activity and cytotoxic effect compared with silver ions. Mater Sci Eng C Mater Biol Appl. 2017;77:963–71. [DOI] [PubMed]
46. Mittal AK, Tripathy D, Choudhary A, Aili PK, Chatterjee A, Singh IP, et al. Bio-synthesis of silver nanoparticles using *Potentilla fulgens* Wall. ex Hook. and its therapeutic evaluation as anticancer and antimicrobial agent. Mater Sci Eng C Mater Biol Appl. 2015;53:120–7. [DOI] [PubMed]
47. Guan Q, Xia C, Li W. Bio-friendly controllable synthesis of silver nanoparticles and their enhanced antibacterial property. Catal Today. 2019;327:196–202. [DOI]
48. Mosaviniya M, Kikhavani T, Tanzifi M, Tavakkoli Yaraki M, Tajbakhsh P, Lajevardi A. Facile green synthesis of silver nanoparticles using Crocus *Haussknechtii Bois* bulb extract: Catalytic activity and antibacterial properties. Colloid Interface Sci Commun. 2019;33:100211. [DOI]
49. Khan S, Shahid S, Sajid M, Noreen F, Kanwal S. Biogenic synthesis of CuO nanoparticles and their biomedical applications: A current review. Int J Adv Res. 2017;5:925–46. [DOI]
50. Rabeea MA, Owaid MN, Aziz AA, Jameel MS, Dheyab MA. Mycosynthesis of gold nanoparticles using the extract of *Flammulina velutipes*, Physalacriaceae, and their efficacy for decolorization of methylene blue. J Environ Chem Eng. 2020;8:103841. [DOI]
51. Wahid Wahab A, Karim A, Asmawati A, Wayan Sutapa I. Bio-Synthesis of Gold Nanoparticles Through Bioreduction using the Aqueous Extract of Muntingia Calabura L. LEAF. Orient J Chem. 2018;34: 401–9. [DOI]
52. Thanh NTK, Maclean N, Mahiddine S. Mechanisms of nucleation and growth of nanoparticles in solution. Chem Rev. 2014;114:7610–30. [DOI] [PubMed]
53. Ansari A, Pervez S, Javed U, Abro MI, Nawaz MA, Qader SAU, et al. Characterization and interplay of bacteriocin and exopolysaccharide-mediated silver nanoparticles as an antibacterial agent. Int J Biol Macromol. 2018;115:643–50. [DOI] [PubMed]
54. Nirmala JG, Akila S, Nadar MSAM, Narendhirakannan RT, Chatterjee S. Biosynthesized *Vitis vinifera* seed gold nanoparticles induce apoptotic cell death in A431 skin cancer cells. RSC Adv. 2016;6: 82205–18. [DOI]
55. Hamelian M, Hemmati S, Varmira K, Veisi H. Green synthesis, antibacterial, antioxidant and cytotoxic effect of gold nanoparticles using *Pistacia Atlantica* extract. J Taiwan Inst Chem Engineers. 2018;93: 21–30. [DOI]
56. Arokiyaraj S, Vincent S, Saravanan M, Lee Y, Oh YK, Kim KH. Green synthesis of silver nanoparticles using Rheum palmatum root extract and their antibacterial activity against Staphylococcus aureus and Pseudomonas aeruginosa. Artif Cells Nanomed Biotechnol. 2016;45:372–9. [DOI] [PubMed]
57. Chauhan B, Dedania J, Mashru DRC. Review on Murraya koenigii: versatile role in management of human health. World J Pharm Pharm Sci. 2017;6:476–93.

58. Nagappan T, Segaran T, Wahid M, Ramasamy P, Vairappan C. Efficacy of carbazole alkaloids, essential oil and extract of Murraya koenigii in enhancing subcutaneous wound healing in rats. Molecules. 2012;17:14449–63. [DOI] [PubMed] [PMC]
59. Abdel-Aziz MS, Shaheen MS, El-Nekeety AA, Abdel-Wahhab MA. Antioxidant and antibacterial activity of silver nanoparticles biosynthesized using *Chenopodium murale* leaf extract. J Saudi Chem Soc. 2014; 18:356–63. [DOI]
60. Saygi KO, Cacan E. Antioxidant and cytotoxic activities of silver nanoparticles synthesized using *Tilia cordata* flowers extract. Mater Today Commun. 2021;27:102316. [DOI]
61. Anbukkarasi M, Thomas PA, Sheu J, Geraldine P. In vitro antioxidant and anticataractogenic potential of silver nanoparticles biosynthesized using an ethanolic extract of Tabernaemontana divaricata leaves. Biomed Pharmacother. 2017;91:467–75. [DOI] [PubMed]
62. Balakrishnan R, Vijayraja D, Jo S, Ganesan P, Su-Kim I, Choi D. Medicinal Profile, Phytochemistry, and Pharmacological Activities of Murraya koenigii and its Primary Bioactive Compounds. Antioxidants (Basel). 2020;9:101. [DOI] [PubMed] [PMC]
63. Ma Q, Xu K, Sang Z, Wei R, Liu W, Su Y, et al. Alkenes with antioxidative activities from Murraya koenigii (L.) Spreng. Bioorg Med Chem Lett. 2016;26:799–803. [DOI] [PubMed]
64. Madubuonu N, Aisida SO, Ali A, Ahmad I, Zhao T, Botha S, et al. Biosynthesis of iron oxide nanoparticles via a composite of Psidium guavaja-Moringa oleifera and their antibacterial and photocatalytic study. J Photochem Photobiol B. 2019;199:111601. [DOI] [PubMed]
65. Mukherjee S, Chowdhury D, Kotcherlakota R, Patra S, B V, Bhadra MP, et al. Potential theranostics application of bio-synthesized silver nanoparticles (4-in-1 system). Theranostics. 2014;4:316–35. [DOI] [PubMed] [PMC]